MDPI

Addendum

SUPPLEMENTARY MATERIAL FOR CELL REPLACEMENT STRATEGIES FOR LITHIUM ION BATTERY PACKS

Nenad G. Nenadic [1†*], Thomas A. Trabold [1†] and Michael G. Thurston [1†]

[1] Rochester Institute of Technology, Rochester, NY 14623, USA
* Correspondence: nxnasp@rit.edu; Tel.: +01-585-662-8250 (N.G.N.)
† These authors contributed equally to this work.

Version July 20, 2020 submitted to Batteries

Abstract: he document provides additional details of the empirical study, such as experimental apparatus and test procedure. The sections are provided as follows: 1) high-level organization of the study, 2) single-cell testing experimental details, 3) pack testing experimental details, 4) divergence of cell characteristics as they age, and 5) additional information on temperature testing.

1. High-level organization

The high-level block diagram of this research program is depicted in Figure 1. It consists of initial characterization, single-cell aging, and aging of cells in a pack. The first step, initial characterization, consisted of measurement of cell weights, their initial capacity during charge, initial capacity during discharge, and impedance spectroscopy at the effective 0% state-of-charge (SOC) and effective 100% SOC. Here we define effective 0% SOC and effective 100% SOC as SOCs that correspond to manufacturer-prescribed minimum and maximum terminal voltages, respectively. As defined, the effective SOCs are current-dependent, viz. the higher the current, the lower the difference between effective 0% and 100% SOC. Since this paper was concerned only with effective SOCs, hereafter they are referred to simply as SOCs.

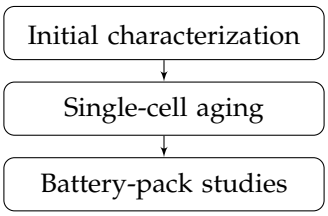

Figure 1. High-level view of the research program.

In the second step, single cell aging, 32 cells were subjected to charge cycling between 0% and 100% SOC using a commercial battery cell tester. In the third step, battery pack studies, cells were aged by cycling them in a pack and comparing based upon the pertinent aging indicators (capacity fade, impedance changes, and relative heating) to the aging indicators of the individually aged cells. After establishing the baseline, a battery pack comprised of individually aged cells and one new cell were then aged to investigate how a mix of new and old cells performs in a pack.

2. Single-cell testing experimental details

The present study employed separate test stands for single-cell and battery pack evaluations. The single-cell apparatus was a Maccor 4600 battery test system, used for initial cell characterization,

pre-aging of individual cells, and periodic monitoring of the cells subjected to pack-level cycling. The process of initial characterization and single-cell aging includes: initial characterization of the as received cells, cycling of the cells to a specified level of capacity degradation, and the final characterization of the tested cell (Figure 2). All the cells were of 18650 type, employing lithium cobalt oxide chemistry, and with Q_n = 2.33 Ah nominal capacity. The received cells were pre-charged to 3.6 V, corresponding to 50% *SOC*.

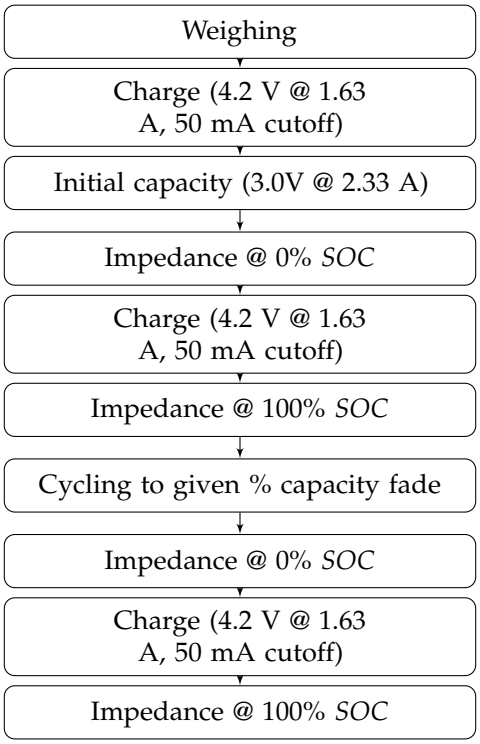

Figure 2. Initial characterization and single-cell testing.

The cells were first weighed, with the results shown in Figure 3. The average mass of 58 cells was 44.26 g, with a small standard deviation of 0.11 g (0.26 %). The fitted Gaussian distribution is indicated in the histogram with dashed lines.

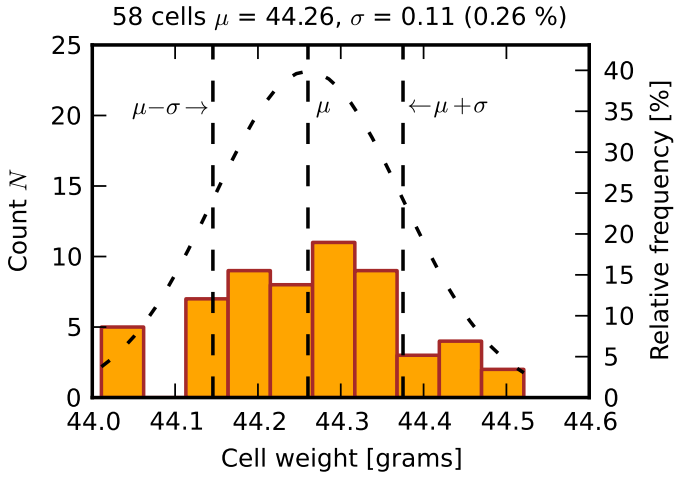

Figure 3. Histogram of cell weights.

Thereafter the cells were charged to 100% SOC at the nominal charge current of I_{Batt} = 1.63 A (0.7 Q_n), using the Maccor single-cell tester. After the initial pre-charge of a cell was complete, the reminder of the initial characterization was as follows:

- cell was first discharged to obtain initial discharge capacity
- impedance spectroscopy scan at 0% SOC
- charged to 100% SOC to obtain the initial charge capacity
- finally, an additional impedance spectroscopy scan was obtained at 100% SOC.

The discharge was performed at 2.33 A (1Q_n) until the terminal voltage dropped down to 3 V. The charge was first conducted in the constant-current mode, at 1.63 A (0.7 Q_n), until the terminal voltage attained 4.2 V. Once the terminal voltage reached 4.2 V, the system switched into constant-voltage mode, viz. the charge current was gradually reduced to zero while maintaining the terminal voltage at 4.2 V.

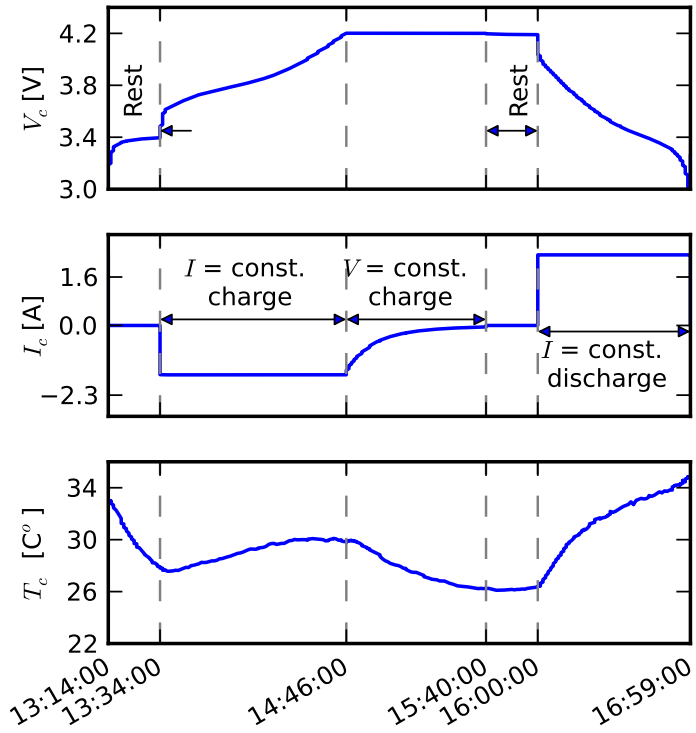

Figure 4. Characteristic waveforms of a typical cycle.

The same charge and discharge profiles were used for cycling the cells on the single-cell tester. Figure 4 shows the characteristic waveforms of one such cycle. During the single-cell cycling, the fixture continuously recorded the characteristic signals as well as accumulated charge. The charge and discharge cycles were separated by 20 minute rest periods. The test was stopped periodically, after about every 20 cycles, to measure the changes in the impedance as the cells aged.

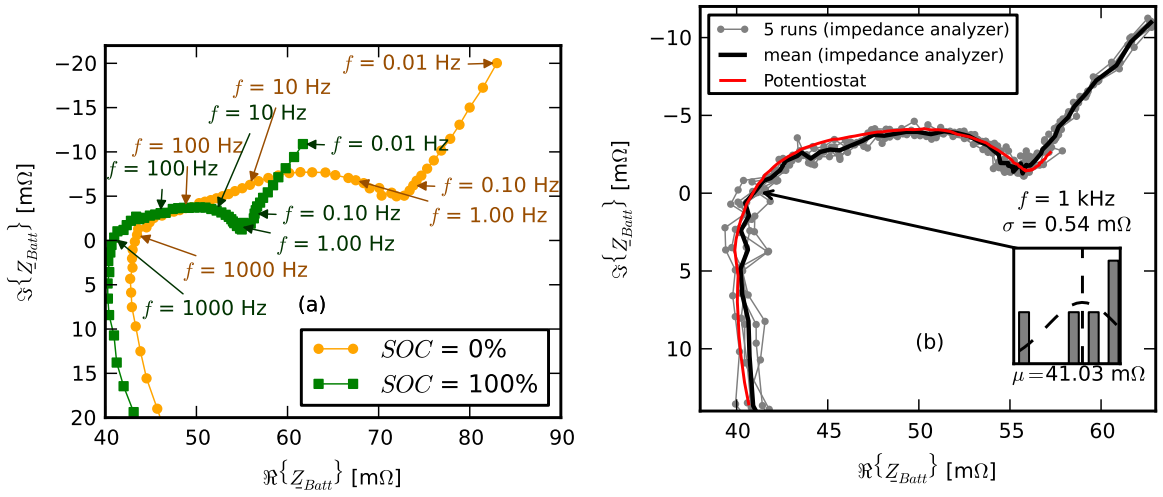

Figure 5. Impedance spectroscopy. (a) Average spectra. (b) Repeatability and potentiostat comparison.

The impedance spectroscopy measurement was performed in the frequency range between 10 mHz and 10 kHz, using a Solartron 1260 impedance analyzer. Figure 5a illustrates a typical impedance plot for a cell at 100% and 0% SOC. Points on the spectrogram trace SOC = 100% are annotated with their corresponding frequencies. The figure shows that the cells exhibited higher resistance at lower state of charge, especially at low frequencies, between 0.01 Hz and 0.1 Hz. While potentiostats are much more commonly used for impedance measurements of low-impedance sources such as batteries, Figure 5b shows that measurements using impedance analyzer, albeit noisier than that of a potentiostat, on average agree well with the potentiostat. Because this study was chiefly concerned with averaged trends, we believe that the measurements obtained with an impedance analyzer are sufficiently accurate for our purposes.

3. Pack testing experimental details

The battery pack experimental configuration was designed in a 3S3P configuration, i.e., three strings connected in parallel, where each string consisted of three cells connected in series (see schematic diagram in Figure 6). The 3S3P pack configuration was chosen because it allowed good observability of charging and discharging of individual cells. In addition, it allowed us to implement charging and discharging profiles that were nearly identical to those employed by the single-cell tester. Figure 7 provides a photograph of the test stand for the battery pack study: Figure 7a shows the complete control, management, and monitoring system, while Figure 7b shows an enlarged photograph of the battery pack itself. The experimental system monitored voltage, current, and temperature of each cell. The pack capacity and energy, as well as capacities and energies associated with each string, were calculated from these measurements, all recorded at 10 second intervals.

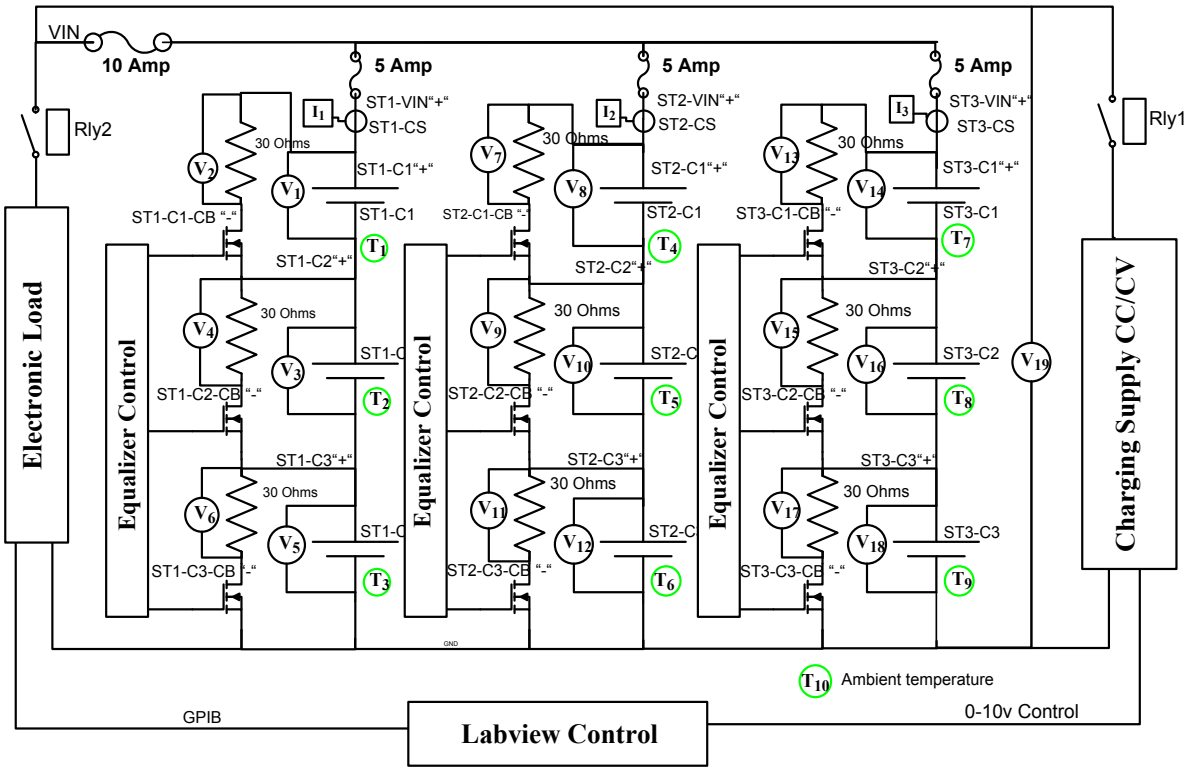

Figure 6. . Schematic diagram of the 3S3P battery pack.

The pack was equipped with a passive cell balancing circuit as illustrated in Figure 7b. When enabled, the circuit could discharge up to 140 mA. The balancing circuit was monitored to determine the amount of energy and charge absorbed during the charge and discharge cycles.

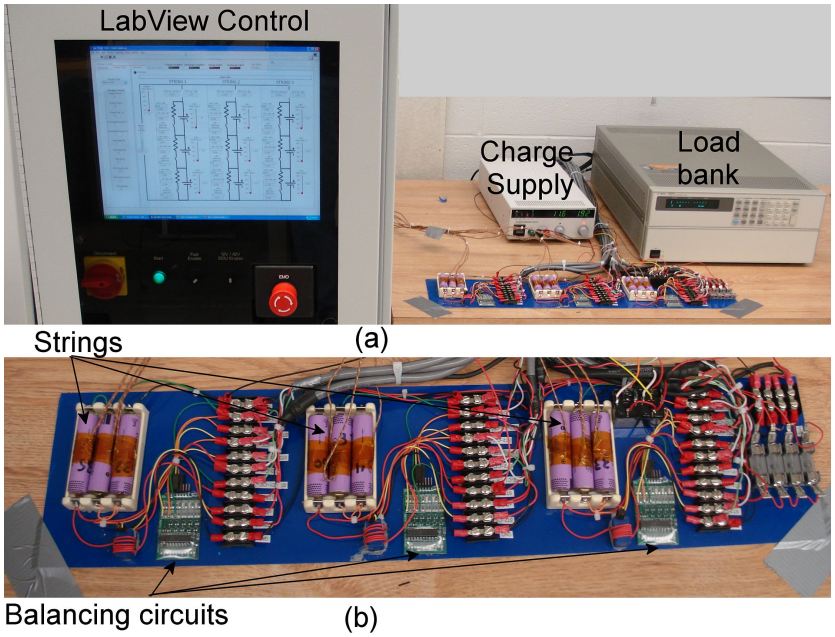

Figure 7. . (a) LabVIEW-controlled battery pack test stand. (b) Enlarged view of the pack

The simple pack was designed based upon the charge/discharge characteristics used in single-cell testing, where the nominal charge current was 1.63 A (0.7 Q_n). The charge cycle started in the constant current mode, with a charge supply current of I_{cs} = 4.89 A, which corresponded to 1.63 A (0.7 Q_n) for

each of the parallel strings, and thereby for each cell. However, in pack charging, a charge management strategy was required to avoid excessive imbalances in cell voltages and string currents. The following pack strategy was used: if the range of string currents exceeded 1 A differential, or the range of the cell voltages exceeded 600 mV differential, the charge supply current was reduced in 250 mA increments until these constraints between the string current and cell voltages were satisfied. The minimum acceptable charge supply current for the pack was 1.2 A. Reducing the charge supply current allowed the cell balancing circuit to equalize the cells. After the current was reduced to the level that led to acceptable imbalances among the string current and cell voltages, it was maintained at that level for 5 minutes. After this 5 minute charge at a reduced current, the system made another attempt to charge the pack at 4.89 A with subsequent step downs in charging current, as needed. The process was repeated until the pack voltage V_{Batt} exceeded 12.6 V, an indication of successful conclusion of the current-controlled state, or until the charge supply current dropped below 2.85 A, an indication of failed charge cycle. If the pack voltage exceeded 12.6 V, the system entered a voltage-controlled state, where the pack voltage was maintained while the current was gradually reduced. Denoting the set of string current by $I_s = \{I_1, I_2, I_3\}$, and the set of cell voltages by V_s= {V_{C1S1}, V_{C2S1}, V_{C3S1}, V_{C1S2}, V_{C2S2}, V_{C3S2}, V_{C1S3}, V_{C2S3}, V_{C3S3}}, a pseudo code of the charge cycle is given in Algorithm 1.

Algorithm 1 Charge cycle

```
# Start current-controlled charging
if min(V_c) ≤ 3 V then
  | I_chargeSupp ← 1.2 A                                   ▷ trickle charge
end
while V_Batt ≤ 12.6 V & I_chargeSupp ≥ 2.85 A do
  | I_chargeSupp ← 4.89A                                   ▷ normal charge
  | #Conditions to fail charge
  | if (max(V_c) ≥ 4.25 or max(T_c) ≥ 50 °C or t_charge ≥ 720 min or min(V_c) ≤ 3 V longer than 120 min) then
  |   | # charge failed
  | end
  | # reduce current if mismatches arise
  | while range(V_s) ≥ 0.6 V or range(I_s) ≥ 1A do
  |   | I_chargeSupp ←max(I_chargeSupp − 0.25A, 1.2A) wait( 5 min )
  | end
end
# Once the total battery voltage exceeds 12.6 V, the charge supply enters voltage-controlled state and
voltage is held at 12.6 V while current is gradually turned off (voltage-controlled charging)
while I_Batt ≥ 80 mA do
  | adjust I_Batt to hold V_Batt at 12.6 V
end
# Charge complete
```

A typical charge cycle took about 4 hours, as shown in Figure 8. The string current I_s fluctuations in the current-control state were indications of the activity in the charge supply regulation process that keeps the imbalances within the prescribed limits. The discharge process was considerably simpler, as the electronic load was set to 7 A until the smallest of the cell voltages dropped to 3 V, viz. min(V_s) ≤ 3 V. Comparing the characteristic waveforms of a cell in a pack during a single cycle (Fig 8) with the characteristic waveforms of cell tested on the single-cell tester during a single cycle (Fig 4) showed that the largest differences occurred in the current signals. During the discharge the sum of the currents was constant, but individual string currents were not constant. During the charge process, care had to be taken to keep the imbalances among cells small.

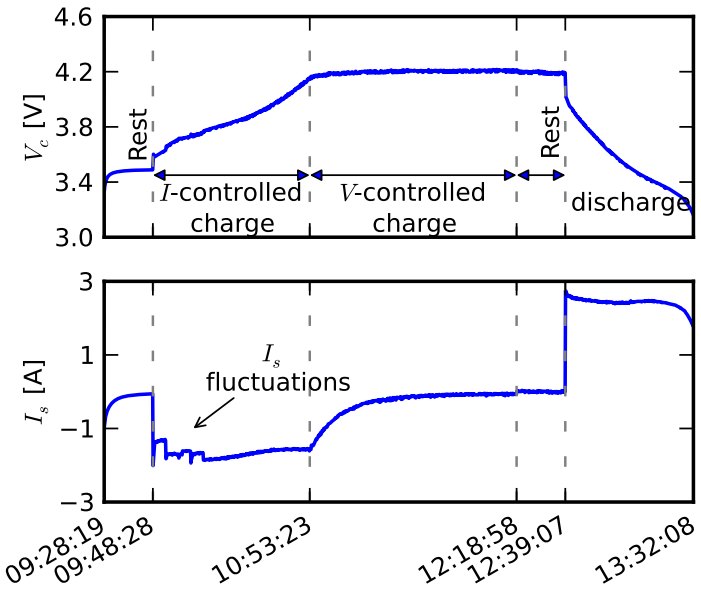

Figure 8. Voltage and current waveforms for a cell during pack cycling.

Figure 9 shows the currents of the three strings for a few charge-discharge cycles. Note that the imbalances were larger during discharge and rests after discharge than during the charges and rests after charges.

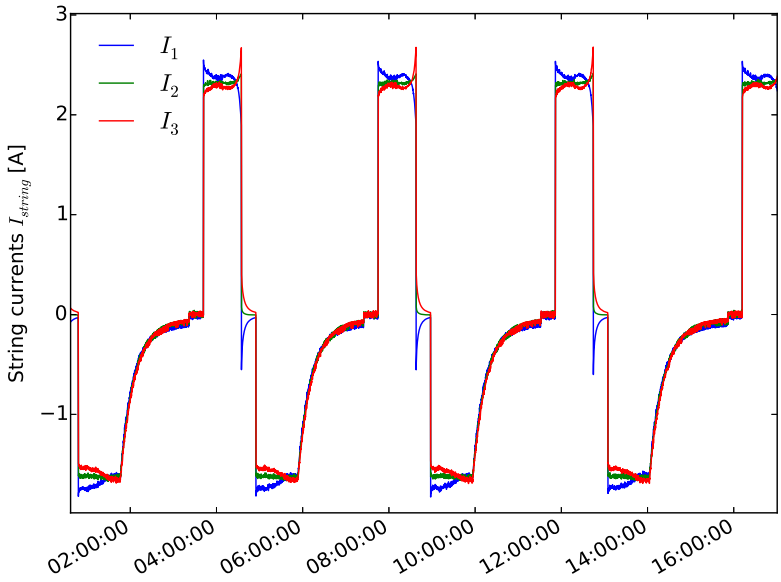

Figure 9. Current distribution of three strings over four cycles.

Figure 10 shows voltages of individual cells of string 1 over four cycles. Note that imbalances after charge were quite small, thanks to passive balancing, while imbalances remained relatively large during the rest after a discharge.

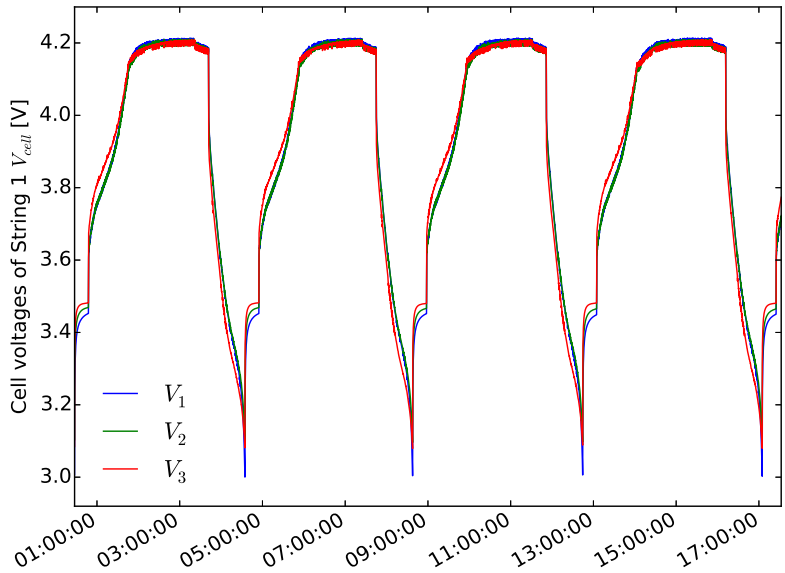

Figure 10. Voltage distribution of three cells within string 1 over four cycles.

At a high level, approaches to cell balancing are classified in two groups: passive and active. Passive balancing dissipates the excess charge, while the active balancing moves the charge via cumulative components (capacitors and inductors). Although more efficient, active cell balancing schemes are less popular due to their greater complexity and thus higher cost. However, for larger size packs, active balancing may be considered to achieve higher efficiency of the pack in the presence of imbalances among cells. This may be particularly important for large packs based on re-purposed cells, such as those planned for grid conditioning. Because of the relative simplicity of the present 3S3P configuration, passive cell balancing was employed first.

The basic principle of operation is illustrated in Figure 11. A series connection of a resistor and a switch was placed in parallel to each cell in a string.

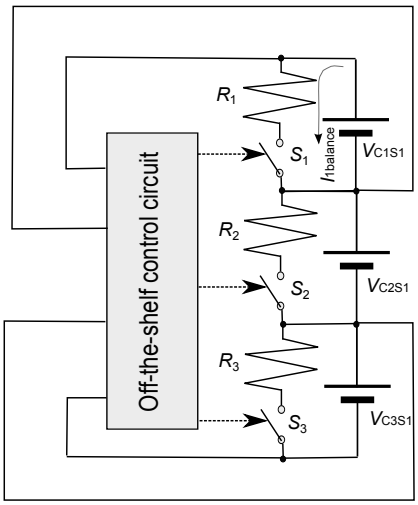

Figure 11. Cell balancing for one of the strings. Pack design employed 106 Astro "Blinky" from AstroFlight Inc. as the commercial cell balancer.

The control circuit monitored individual cell voltages and, in case of excessive imbalance, shorts the switch parallel to the cell of the highest voltage. The balancing current, being the ratio of the cell voltage and the resistor, e.g.,

$$I_{1balance} = \frac{V_{C1S1} - V_{S1}}{R_1} \quad (1)$$

was limited. For our circuit, equipped with 30 Ω resistors and cell voltages in the 3.0 - 4.2 V range, ignoring the voltage drop across the switch, the balancing current was in the [100, 140] mA range.

Active cell balancing switched a balancing 1F capacitor across individual cell at f = 1f Hz. Figure 12 shows individual cell voltages in a string over four cycles.

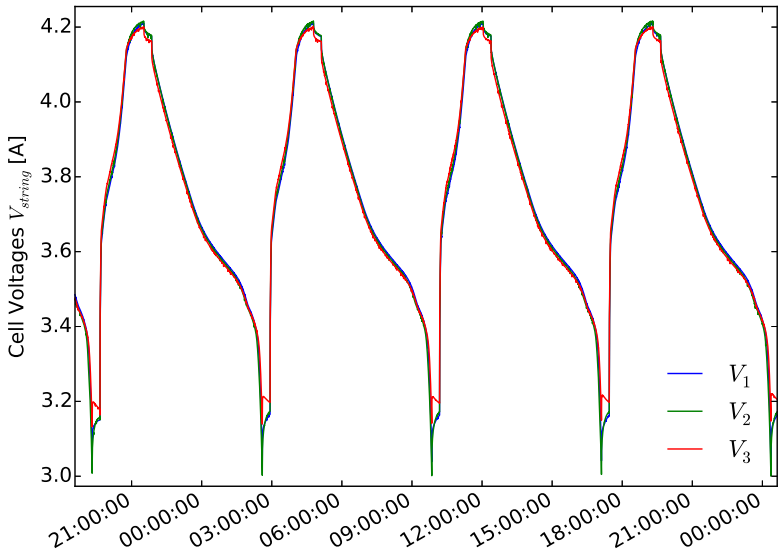

Figure 12. Voltage distribution of three cells within string 1 over four cycles for active cell balancing.

4. Divergence of cell characteristics as they age

One of the main concerns in building packs using repurposed cells is divergence of cell characteristics. These mismatches grow as the cells age, as illustrated in Figure 13a showing capacity of individually aged cells. In this plot different cells were aged using the same profile on the individual cell tester described in Section 1 of this document. The traces are labeled with identification numbers of individual cells. Although the cells were rested for twenty minutes after each charge/discharge cycle, consistent discontinuities in the fading capacities occurred after longer, one day rest periods. During these longer rest periods impedance measurements were taken. The benefits of longer rest periods was proportional to capacity fade. The relationship between the magnitude of the recovery and the capacity fade is seen in the scatter plot of Figure 13b, which shows cell capacity in % of nominal capacity vs. the magnitude of the recovery, denoted by ΔQ_c, also expressed in percent of the nominal capacity. The linear model of the relationship fitted by least squares is indicated in the plot with the black dashed line. The associated correlation coefficient was $\rho \approx$-0.9.

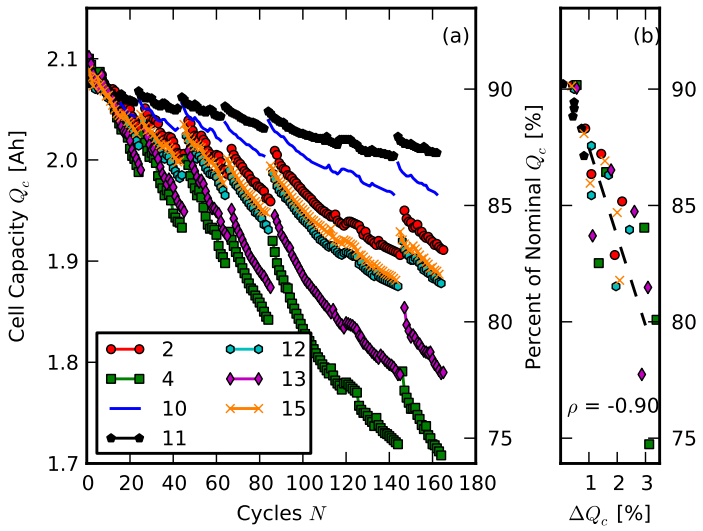

Figure 13. (a) Representative capacity of individual cells diverging in time (18650, lithium cobalt oxide chemistry). (b) Scatter plot of capacity fade vs. percent recovery

It is important that this aging divergence is more pronounced than typical aging of cobalt based chemistries because cells from a less rigorous quality control manufacturer were used. More typically, this divergence takes place much later. For comparison, Figure 14 shows aging of cell from the same family, but of significantly better quality. Here the divergence took place much later and it was less pronounced.

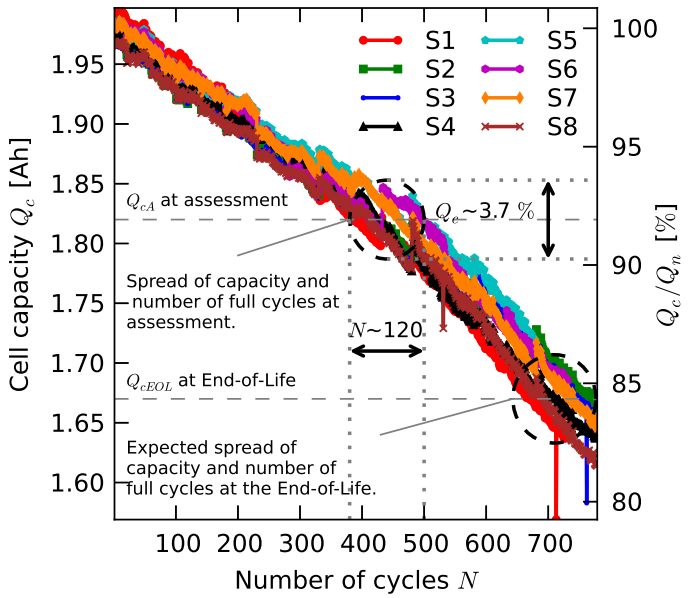

Figure 14. Capacity fade of eight lithium cobalt cells.

Figure 14 shows natural capacity degradation of eight lithium cobalt cells, labeled S1 through S8, subjected to full cycle charges and discharges vs. the number of cycles N. The circles indicate the in-class spread of the data in Q_c-N space. The spread slightly increases as the cells age.

5. Additional information on temperature testing

For a given cycle, cell temperature T_c was maximized at the end of discharge T_{ed} (refer to Figure 4a of the main paper). It was observed that T_{ed}'s are correlated to the ambient temperature (Figure 4b of the main text).

Table 1 shows correlation coefficient between of ambient temperature T_a and T_{ed} of sixteen cells. In addition, the table includes the coefficient for linear fit: offset a_0 and slope a_1.

Table 1. Effect of T_a on T_{ed} .

	Correlation coefficient	Linear coefficients	
Cell ID 1	ρ	a_0 [^{o}C]	a_1 [.]
1	0.953	1.61	-2.63
2	0.983	1.71	-6.03
3	0.890	1.40	-1.94
4	0.970	1.74	-8.75
5	0.919	1.24	2.34
6	0.976	1.12	5.39
7	0.988	1.46	-2.37
8	0.975	1.16	4.58
9	0.996	1.25	0.73
10	0.992	1.12	4.21
11	0.945	1.01	7.80
12	0.961	1.09	4.25
13	0.983	1.01	7.32
14	0.964	0.97	7.43
15	0.894	0.96	9.14

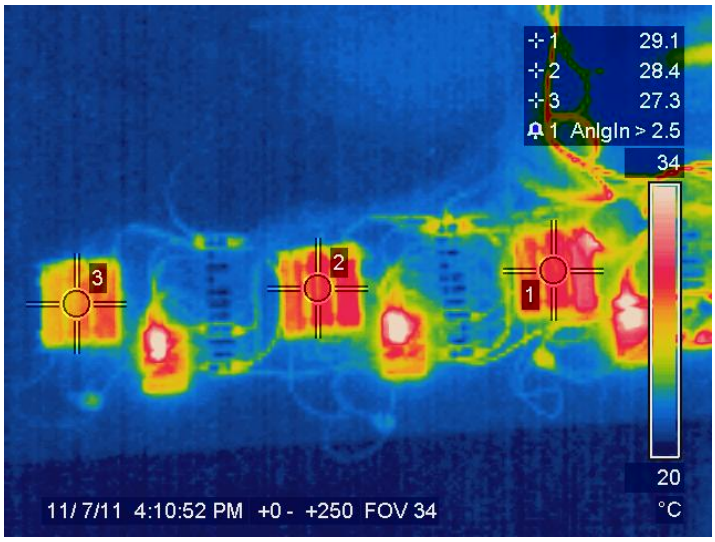

Figure 15. Thermal image of the pack.

Figure 15 shows the thermal image of the pack at the end of discharge, when the cells' temperature was highest. The hot spots (appearing as white regions in the image) of the pack were typically not the cells themselves, but some of the electronics components. In this pack the cells were not in direct contact and they could radiate heat to the environment. The temperature across a cell was relatively uniform. During all the pack testing, each cell was equipped with a thermocouple. These sensors were used to determine temperature behavior of the three packs and enable their comparisons.

Figure 16 shows an alternative view of temperature histograms to that of Figure 16 of the main paper. Here the bottom plot shows the entire time domain traces of the three temperature differences. Again, we see that the maximum temperature difference did not correspond to most recent cycles.

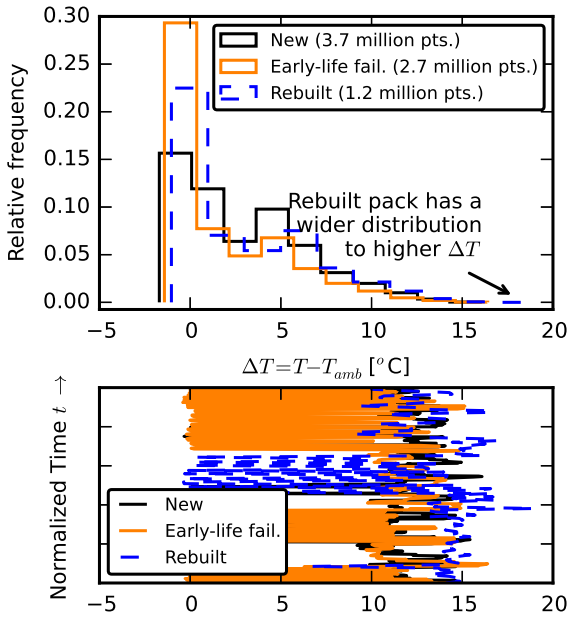

Figure 16. Comparison of heating of lithium ion batteries.